small
NANO MICRO
www.small-journal.com

In Situ Probing of the Particle-Mediated Mechanism of WO_3-Networked Structures Grown inside Confined Mesoporous Channels

Lingling Zhang, Jiang Li, Hongjun You, Chuansheng Ma, Si Lan,* Zhenduo Wu, Jianrong Zeng,* Feng Tian, and Jixiang Fang**

Nanocasting, using ordered mesoporous silica or carbon as a hard template, has enormous potential for preparing novel mesoporous materials with new structures and compositions. Although a variety of mesoporous materials have been synthesized in recent years, the growth mechanism of nanostructures in a confined space, such as mesoporous channels, is not well understood, which hampers the controlled synthesis and further application of mesoporous materials. Here, the nucleation and growth of WO_3-networked mesostructures within an ordered mesoporous matrix, using an in situ transmission electron microscopy heating technique and in situ synchrotron small-angle X-ray scattering spectroscopy, are probed. It is found that the formation of WO_3 mesostructures involves a particle-mediated transformation and coalescence mechanism. The liquid-like particle-mediated aggregation and mesoscale transformation process can occur in ≈10 nm confined mesoporous channels, which is completely unexpected. The detailed mechanistic study will be of great help for experimental design and to exploit a variety of mesoporous materials for diverse applications, such as catalysis, absorption, separation, energy storage, biomedicine, and nanooptics.

An understanding of nanocrystal growth mechanisms is essential for the controlled synthesis of nanocrystals and their good performance in applications. Based on the model proposed by LaMer and improved by Reiss,[1,2] "size distribution focusing" can be exactly controlled by adjusting the monomer concentration. The introduction of an organic molecule that selectively adheres to a particular crystal facet can be used to tailor the anisotropic growth of nanocrystals, creating a variety of shapes.[3] However, these models were the only possibility for nanocrystal growth through the addition of monomeric species (i.e., atoms or molecules). In 1998, Penn et al. proposed an important crystal growth mechanism called "oriented attachment" (OA), which is a particle-mediated growth process in which nanocrystals collide and form loose aggregates.[4] Recently, particle–particle interactions have been examined in diverse reaction systems using in situ transmission electron microscopy (TEM) under operating conditions with atomic and time resolution.[5,6] This new nanocrystal growth mechanism contributes to the formation of a fascinating class of materials, called "mesocrystals,"[7–9] and the preparation of a large number of anisotropic structures and complex hierarchical nanostructures.[10–12]

Since the discovery of ordered mesoporous silicas, interest in this field has rapidly expanded to various mesoporous materials with different compositions, such as carbons, metals, metal oxides, and sulfides.[13] Owing to their fascinating physicochemical properties, including high porosity, large specific area, tunable pore size, and narrow pore-size distribution, mesoporous materials offer a wide range of promising applications in catalysis, absorption, separation, energy storage, drug delivery, and nanooptics.[14] Currently, template synthesis is a popular approach for preparing nanoporous materials with various porous structures. However, the synthesis of well-controlled monodisperse nanoparticles (NPs) with narrow size distribution via nanocasting using ordered mesoporous materials as templates remains largely unexplored,[15] seriously hampering applications of the materials. This is partially because the growth mechanism in a confined space remains unclear. In addition, NPs dispersed on a mesoporous carrier are widely used as solid catalysts.[16] However, the tendency of supported NPs to grow into larger crystallites through a ripening mechanism is a major cause of deactivation for supported catalysts. Therefore, in recent studies, much effort has been devoted to

L. L. Zhang, J. Li, Prof. H. J. You, Dr. C. S. Ma, Prof. J. X. Fang
Key Laboratory of Physical Electronics and Devices of Ministry of Education
School of Electronic and Information Engineering
Xi'an Jiaotong University
Xi'an, Shann xi 710049, China
E-mail: hjyou@mail.xjtu.edu.cn; jxfang@mail.xjtu.edu.cn
Prof. S. Lan, Prof. Z. D. Wu
Herbert Gleiter Institute of Nanoscience
School of Materials Science and Engineering
Nanjing University of Science and Technology
Nanjing 210094, China
E-mail: lansi@njust.edu.cn
Dr. J. R. Zeng, Prof. F. Tian
Shanghai Synchrotron Radiation Facility
Shanghai Institute of Applied Physics
Chinese Academy of Sciences
Shanghai 201204, China
E-mail: zengjianrong@sinap.ac.cn

DOI: 10.1002/smll.201702565

understanding the sintering behaviors of NPs to prevent catalyst deactivation via in situ characterizations.[17–19]

Understanding the physical mechanism, including filling, diffusion, migration, aggregation, and coalescence, inside mesoporous templates during nanocasting, reduction processes, and thermal treatment is vital to obtain a controlled synthesis and further applications, such as catalytic reactions.[20] However, gaining deep insight into the entire reaction process and mechanism in a confined mesoporous template remains a significant challenge. Herein, taking the WO_3 precursor decomposition reaction inside a KIT-6 mesoporous template for example, for the first time, we report the processes and mechanism involved in precursor decomposition and the aggregation and coalescence of WO_3-networked nanostructures using an in situ TEM heating technique and in situ synchrotron small-angle X-ray scattering spectroscopy (SAXS).

By means of a typical impregnation process, $H_3PW_{12}O_{40}\cdot nH_2O$ was absorbed by a KIT-6 mesoporous silica template. A typical TEM image of the WO_3 precursor immersed in the SiO_2 template is shown in **Figure 1**b, displaying that the WO_3 precursor is relatively uniformly distributed over the entire silica matrix. However, some fine NPs or NP aggregates are clearly observed. In the following, WO_3-networked nanostructures can be formed via a calcination route under various temperatures in air (Figure 1a). Figure 1c shows the TEM image of WO_3 networks dispersed in the silica matrix, demonstrating a well-replicated structure of the KIT-6 hard template. The TEM images in Figure S1 (Supporting Information) show that large-sized mesopores of around ≈18 nm are created, corresponding to the total wall thickness plus the pore size of KIT-6. This square-shaped network structure indicates that the mesoporous AuAg NPs replicate one side of the pore system in the bicontinuous structure[21,22] In addition, the single mesostructural Ia 3d domain of the original KIT-6 (red arrows) and WO_3 structures with various dimensions (e.g., 3D or 1D) are also obtained, as shown in Figure S1 (Supporting Information), which further supports that well-replicated WO_3 structures were obtained. Finally, dispersed WO_3 nanostructures can be obtained by removing the silica template using hydrofluoric acid, as shown in Figure 1d and Figure S2 (Supporting Information). In particular, the SAED pattern in Figure 1e indicates that the individual WO_3 NPs have a single-crystal structure. The TEM images observed from different angles support that the WO_3 NPs have a 3D networked structure (Figure S3, Supporting Information). The XRD pattern (Figure S4, Supporting Information) of the WO_3 NPs obtained after calcination at ≈550 °C shows that the WO_3 product is mainly in the orthorhombic phase.

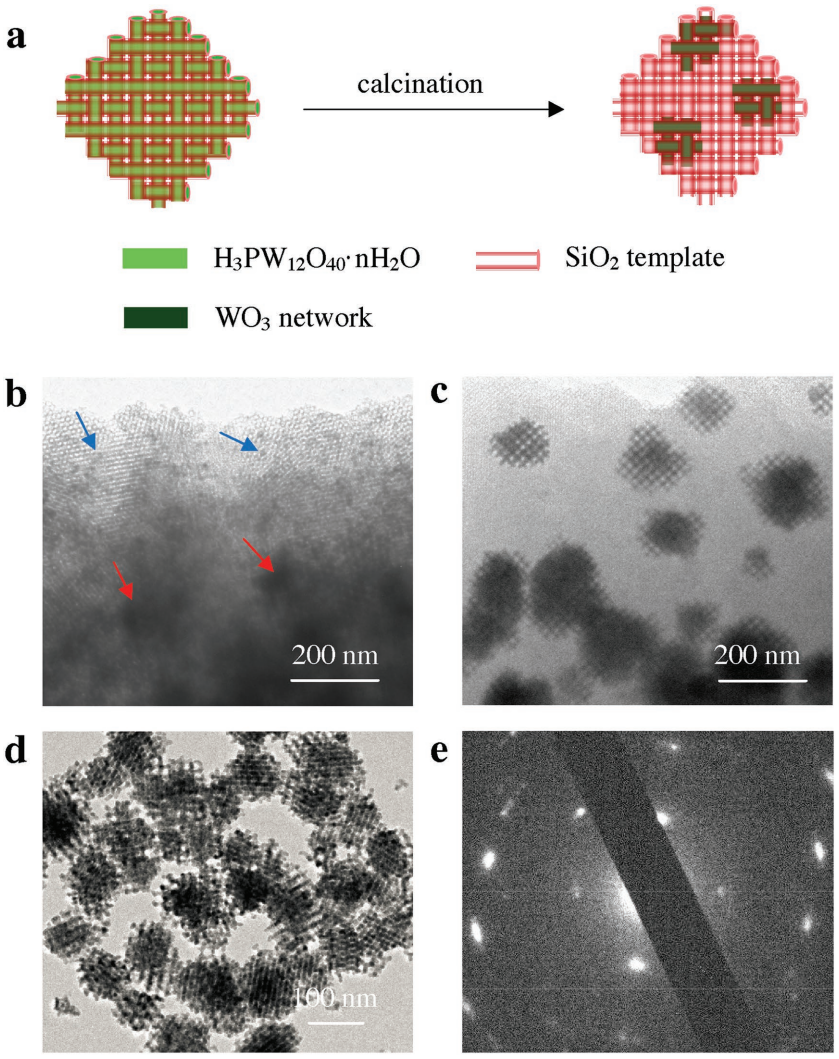

Figure 1. Schematic illustrations of the preparation of WO_3 mesoporous networked nanostructures via calcination of WO_3 precursor. a) The schematic transformation from WO_3 precursor to WO_3 mesoporous networks. b) The TEM image of WO_3 precursor immersing into silica matrix, and the blue and red arrows represent dispersed fine NPs and NP aggregations, respectively. c) WO_3 mesoporous networks immersing into silica matrix. d,e) The TEM image and SAED pattern of WO_3 mesoporous networks. The SAED pattern showing the single-crystal essence of individual WO_3-networked NPs.

To investigate the formation and growth mechanism of WO_3-networked nanostructures, a variety of quasi-in situ and in situ TEM heating measurements were carried out. When the heating was performed under vacuum, the WO_3 precursor did not change even at heating temperatures up to 850 °C. No obvious mass migration and coalescence were observed (Figures S5 and S6, Supporting Information). As a result, the mesoporous-networked WO_3 nanostructures cannot be formed via calcination under vacuum. This is a remarkable difference compared with metal-component reaction systems, where metal NPs can migrate inside/between channels in the mesoporous template even during heating under vacuum.[19] In fact, previous studies suggest that the sintering of metal NPs

dispersed on either planar model or porous technical-relevant alumina supports is strongly promoted by exposure to oxygen at temperatures above ≈500 °C, and other components of the diesel exhaust, such as nitrogen oxides and CO, may also affect the sintering of the catalyst.[23] Therefore, considering that WO_3-networked NPs were formed by heating in air, in the following, we carried out in situ TEM observations by exposing the WO_3 precursor to air at elevated temperatures.

Figure 2 presents the typical configurations of WO_3 nanostructures calcinated at different temperatures. When the WO_3 precursor is heated from 25 to 400 °C, the TEM images indicate no obvious mass diffusion or migration (Figure S7, Supporting Information). In this situation, many fine NPs and aggregations disperse into the entire silica matrix (Figure 2a,d). As the heating temperature increases, e.g., up to 450–470 °C, the contrast in the TEM image becomes faint owing to the volume shrinkage along with reduced mass transport (Figure 2b,e; Figure S8a,b, Supporting Information). When the calcination temperature approaches ≈500 °C, the contrast in the TEM image begins to increase, and remarkable mass transport occurs. In this case, the numerous fine NPs thoroughly vanished by means of diffusion, migration, and reaggregation. As a result, an increasing amount of larger NP aggregates was observed (Figure 2c,f; Figure S5c, Supporting Information). Comparing the image in Figure 2f with that in Figure 2e gives a strong indication of fine NP diffusion and migration on a wide scale and over a long distance. In addition, no larger WO_3 NPs can be found on the surface of the silica template, indicating that the diffusion and migration of fine NPs occurred only in the interior of the mesoporous channels. Unlike the WO_3 reaction system, in a comparison experiment, Au NPs were easily expulsed and rejected from the mesopores when heating $HAuCl_4$ and the mesoporous silica compound (Figures S9 and S10, Supporting Information).

When the calcination temperature was further increased from 500 to 550 °C, the contrast in the TEM images was increased further (**Figure 3**a,b; Figure S8c,d, Supporting Information). In addition to the further diffusion and migration of fine NPs, larger NPs can also move and reposition (Figure S7c,d, Supporting Information). Finally, increasingly monodispersed WO_3-networked NPs appear. It is also worth noting that the initial loose aggregates (Figure 3c) formed at ≈500 °C were converted into an ordered networked structure (Figure 3d), revealing the occurrence of a coalescence and densification process during this period. To investigate structural changes during the coalescence and densification process, calcination temperature-dependent SAED patterns were measured (Figure S11, Supporting Information). It was found that the loose aggregates typically demonstrate a polycrystalline or quasisingle crystalline pattern (Figure 3e–i). As the temperature increases from 470 to 550 °C, the SAED patterns display an observable evolution from quasisingle crystal to single crystal.

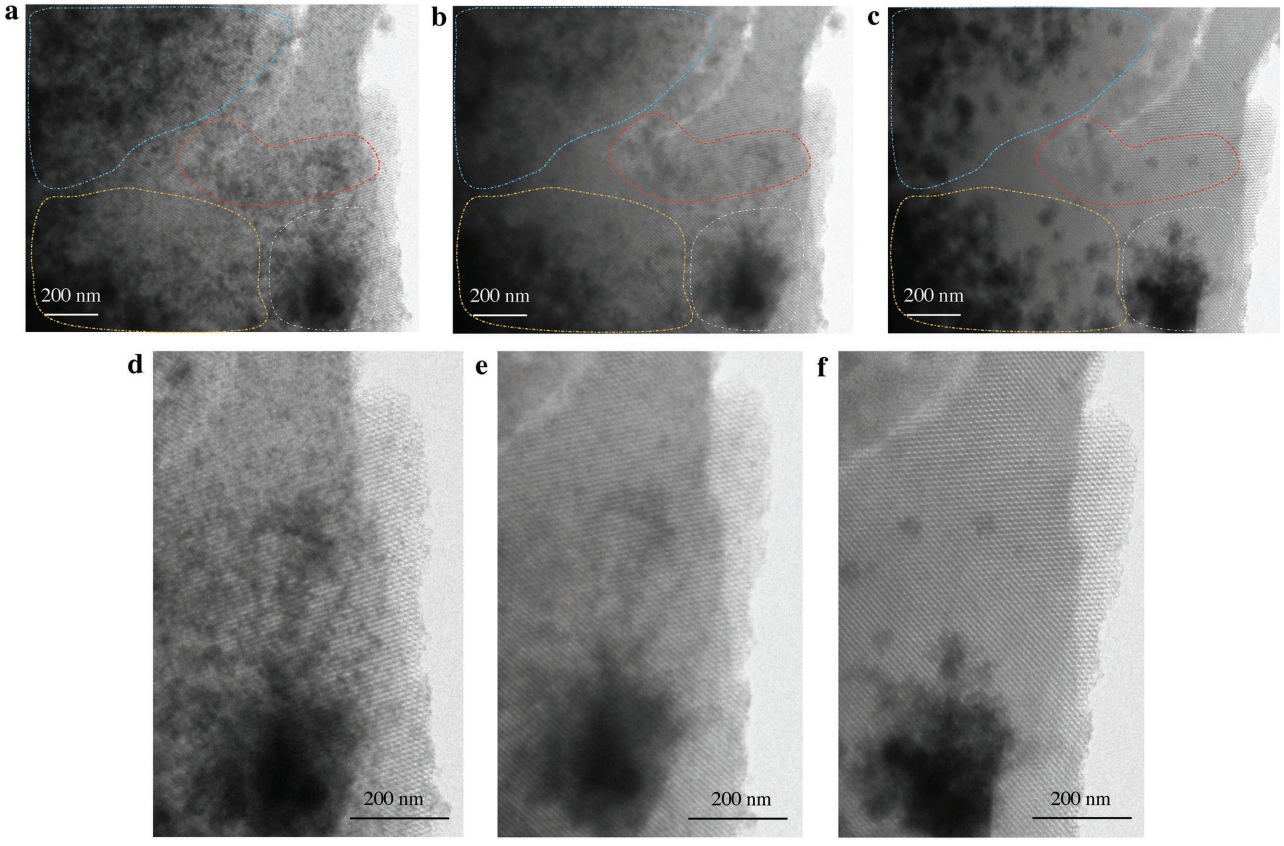

Figure 2. TEM images of a series of WO_3 nanostructure/silica composites with different configurations under in situ TEM calcination at different calcination temperatures: a) 400 °C, b) 470 °C, and c) 500 °C. The different color regions represent different NP configurations. d–f) The magnified regions of (a–c) indicating the diffusion and migration of WO_3 NPs.

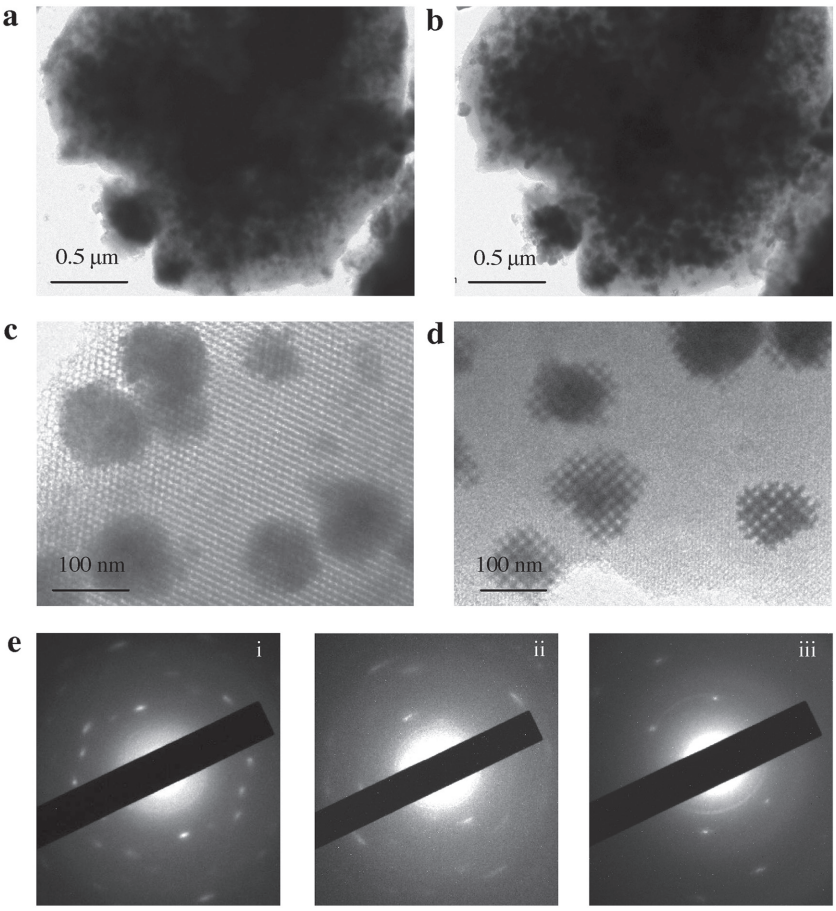

Figure 3. TEM images of WO_3 nanostructure/silica composites with different configurations under in situ TEM calcination at different calcination temperatures: a) 500 °C, b) 550 °C, and c,d) the magnified regions of WO_3 nanostructures calcinated at 500 and 550 °C. e) The SAED patterns obtained from individual WO_3 nanostructures from 470 to 500 to finally 550 °C, respectively. The SAED patterns show an evolution from quasisingle crystal to finally single crystals.

To unambiguously assess the number and size distribution of the WO_3 NPs, in situ SAXS measurements were performed during the calcination process since SAXS is an effective technique for obtaining statistical information over the entire specimen. **Figure 4**a shows the SAXS profiles at different temperatures of WO_3 NPs/KIT-6 upon in situ heating (Figure S12, Supporting Information). As a control, the SAXS profiles of pure KIT-6 upon in situ heating at different temperatures are also illustrated in Figure 4b (Figure S13, Supporting Information). The low-angle diffraction peaks between 0.6 and 1 nm^{-1} can be attributed to the periodic structure of KIT-6. The SAXS profile of WO_3 NPs/KIT-6 displays two scattering features at low-angle regions below ≈0.6 nm^{-1} in comparison with the SAXS profile of the pure KIT-6 sample. First, there is an additional low-angle diffraction peak at ≈0.4 nm^{-1}, indicated by the blue arrow, corresponding to the periodic networked nanostructure[23] of the WO_3 NPs. The observation of the networked nanostructure can be confirmed by TEM images, as shown in Figure 3d. The diffraction peak at ≈0.4 nm^{-1} is observable at lower temperatures and becomes sharp upon heating above ≈430 °C. Figure 4c shows the integrated intensity of the low-angle diffraction peak between 0.32 and 0.42 nm^{-1}. There is a rapid intensity increase above ≈430 °C. The sharpening process and the increase in relative intensity indicate that the WO_3 NPs experience a transition from the "polycrystalline-like" or "disordered-like" state at the very beginning to a more ordered state[24] at the end of the calcination process. Figure 4d displays the change in the peak position of the low-angle diffraction peak at ≈0.4 nm^{-1} with temperature. The peak position suddenly shifts to the high q position above 430 °C, indicating that the characteristic length of the periodic networked nanostructure of the WO_3 NPs decreases upon heating. The shrinkage of the networked nanostructure is consistent with the densification of the WO_3 NPs. **Figure 5**e shows the pair distance distribution function (PDDF) of the WO_3 particles at 550, 570, and 590 °C, obtained from the Fourier transform of the SAXS data over a q range from 0.02961 to 0.2073 nm^{-1} using the IGOR software equipped with the IRENA macro. At temperatures below 530 °C, there is no apparent Guinier shoulder over a q range below 0.3 nm^{-1}, as shown in Figure 4a. Therefore, PDDF analysis was performed for the SAXS profiles obtained at temperatures above 530 °C. The distribution profile of the WO_3 NPs at 550 °C is broad and covers a large range due to the formation of polydisperse NPs. Upon heating, the polydispersity of the size distribution of the WO_3 NPs continues to decrease. Finally, the system tends to form monodisperse WO_3 NPs with narrow size distribution, as indicated by the PDDF profile at 590 °C in Figure 4e. It is noted that the TEM observations and SAXS measurements of the heating-temperature-dependent structural evolution of the WO_3 NPs are slightly different. This may be due to the high heating speed of SAXS. However, the experimental results and corresponding conclusions obtained from the TEM observations and SAXS measurements are highly consistent.

According to the above observations, valuable insights into the formation mechanism can be derived from the in situ characterizations of the formation of the WO_3-networked structure. Our findings may have particular implications in that the formation of WO_3-networked NPs involves a particle-mediated mesoscale transformation and coalescence mechanism. This statement is nicely supported by the results obtained from density functional theory (DFT) calculations. First, we evaluated the capability of a WO_3 molecule to detach from the WO_3 cluster and WO_3 cluster movement on the SiO_2 surface by breaking the corresponding chemical bonds when exposed to air or vacuum conditions (Figure 5). Previous studies suggest that oxygen atmosphere may affect the surface free energy and thus the sintering behavior.[25] In this study, when the reaction was exposed to air, the oxygen molecules in air are adsorbed on the surface

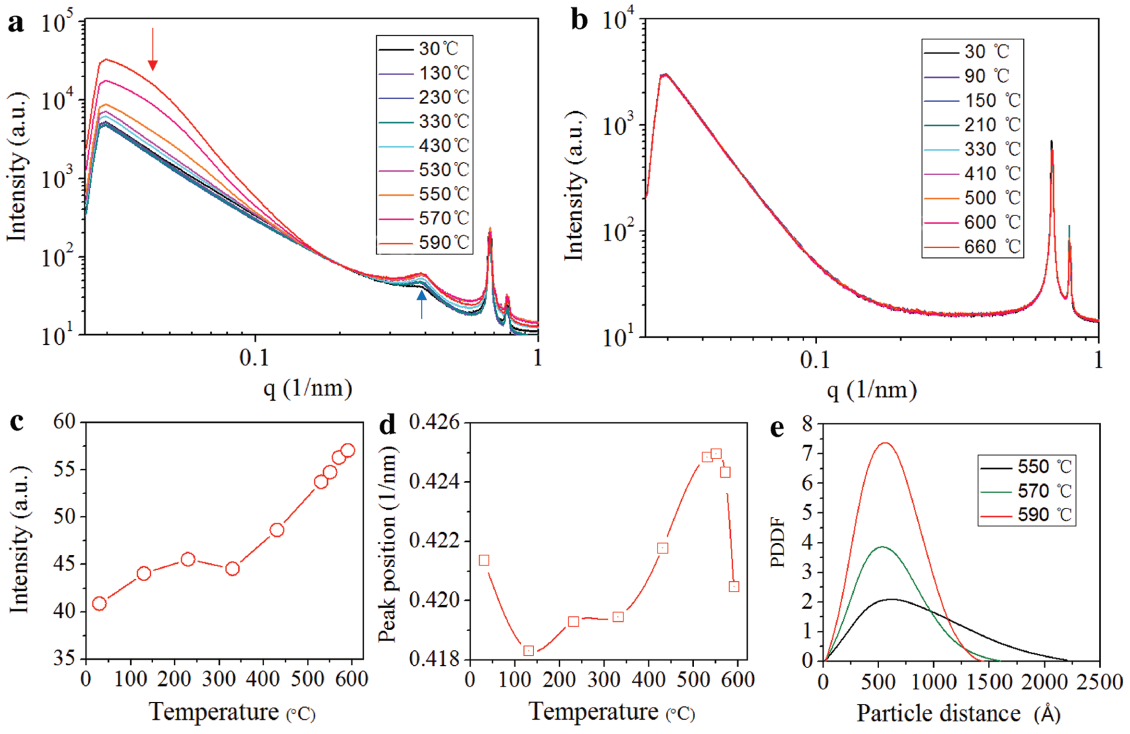

Figure 4. In situ SAXS measurement for the growth for WO_3 NPs during the calcination process. a) SAXS profiles at different temperatures of WO_3 nanostructures/KIT-6 upon in situ heating. The red arrow indicates the Guinier shoulder that belongs to the size distribution of WO_3 NPs. The blue arrow indicates the low-angle diffraction peak for the networked nanostructure of the WO_3 NPs (clusters). b) SAXS profiles at different temperatures of KIT-6 upon in situ heating. c) Integrated intensity of the low-angle diffraction peak at ≈0.4 nm^{-1} as indicated by the blue arrow. The integration q range is between 0.32 and 0.42 nm^{-1}. d) Peak position of the low-angle diffraction peak at ≈0.4 nm^{-1} of different temperatures upon heating. e) The PDDF of WO_3 particles at 550, 570, and 590 °C. PDDF was obtained by indirect Fourier transform (IFT) of the SAXS data at q range from 0.02961 to 0.2073 nm^{-1}.

of the SiO_2 substrate (Figure 5ai), reducing the activation barrier for WO_3 molecules to detach from the SiO_2 surface via molecule rotation (Figure 5aii). In this situation, the molecular rotation of WO_3 via breaking the W—O and O—O bonds must overcome a relatively low energy barrier of 0.11 eV (Figures S14 and S15, Supporting Information). When the reaction occurs

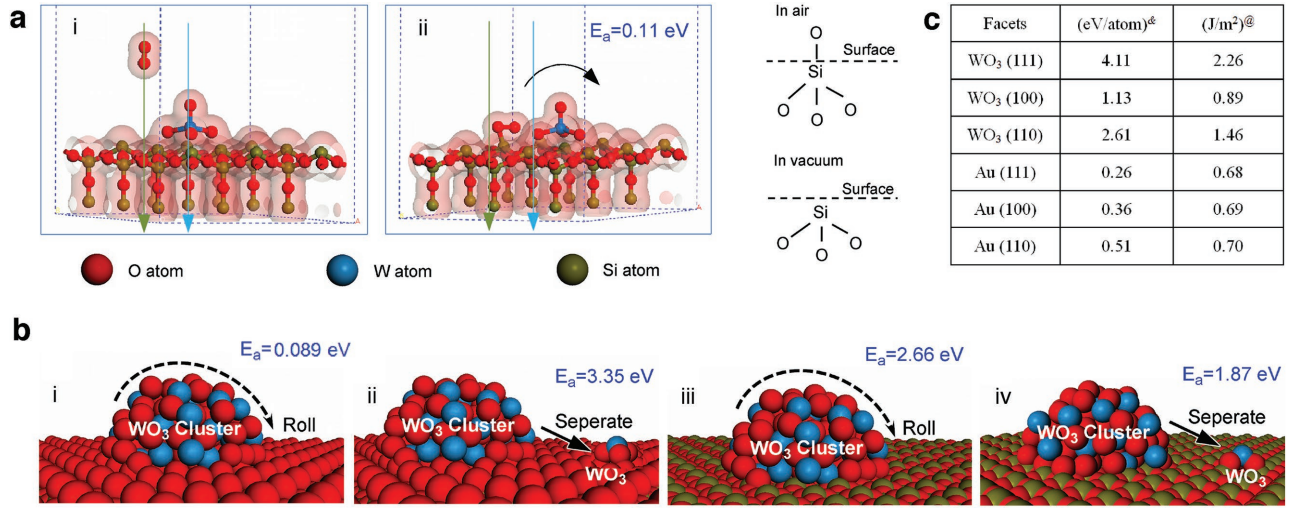

c

Facets	(eV/atom)[&]	(J/m²)[@]
WO_3 (111)	4.11	2.26
WO_3 (100)	1.13	0.89
WO_3 (110)	2.61	1.46
Au (111)	0.26	0.68
Au (100)	0.36	0.69
Au (110)	0.51	0.70

Figure 5. Activation barriers and surface energies obtained by DFT calculations. ai) The model of introducing an oxygen molecule to the reaction system where WO_3 molecule absorption on SiO_2 surface. aii) The optimized results of model (a), displaying the WO_3 molecule may rotate via breaking the corresponding chemical bonds as a function of oxygen introduction. b) The different calculated results including i) WO_3 cluster rotates on oxygen-abundant SiO_2 surface, ii) WO_3 molecule detaching from WO_3 cluster on oxygen-abundant SiO_2 surface, iii) WO_3 cluster rotates on SiO_2 surface, and iv) WO_3 molecule detaching from WO_3 cluster on SiO_2 surface. c) The calculated surface energy for the WO_3 and Au reaction system. The superscripted symbol & represents the surface energy per atom and @ represents the surface energy per surface area, respectively.

in air at elevated temperatures, e.g., 400 °C, the SiO_2 surface may be attacked by more oxygen molecules. The interaction between a WO_3 cluster and three oxygen atoms of the SiO_3 surface is extremely weak (Figure S16, Supporting Information) such that the electron cloud does not even overlap. In this case, the energy barrier of WO_3 molecular rotation can be further reduced to 0.089 eV. However, in an oxygen-abundant atmosphere, the energy barrier for the detachment of a WO_3 molecule from the WO_3 cluster, as shown in Figure S17 (Supporting Information), is 3.35 eV (Figure 5bii). The comparison of Figure 5bi,ii indicates that WO_3 cluster migration is much easier than the detachment of a WO_3 molecule from the WO_3 cluster. That is, when the reaction occurs in air, WO_3 cluster migration is the dominant process during the WO_3 nanocrystal growth.

For comparison, we also investigated WO_3 cluster movement under vacuum and the Au cluster behavior on the SiO_2 surface via DFT calculations. When WO_3 NPs are grown under vacuum or on an oxygen-deficient SiO_2 surface, the electron cloud between the WO_3 cluster and SiO_2 surface obviously overlaps, revealing the existence of a strong interaction (Figure S18, Supporting Information). In this case, the energy barriers of WO_3 cluster movement on the SiO_2 surface and the detachment of a WO_3 molecule from the WO_3 cluster are 2.66 and 1.87 eV, respectively (Figure 5biii,iv; Figure S19, Supporting Information). Compared to the oxygen-abundant atmosphere, it is reasonable to state that WO_3 molecules do not easily diffuse, migrate, or aggregate on an oxygen-deficient SiO_2 surface or under vacuum. Therefore, as determined by the experiments, networked WO_3 nanostructures cannot be formed under vacuum (Figures S5 and S6, Supporting Information). In addition, we also calculated the activation energy of Au cluster growth within a silica template, including Au cluster movement or Au atom detachment from the Au cluster. It was found that the activation energies of both cases are similar regardless of the presence or absence of oxygen (Figures S20–S24, Supporting Information). This reveals that both the particle-mediated and atom-mediated growth mechanisms contributed to the growth of Au nanostructures. The two growth mechanisms indeed have been reported in previous experiments.[26] However, the other remarkable distinction between the WO_3 and Au reaction systems is that Au nanostructures can be rejected from the mesochannels, while WO_3 can grow completely inside the mesoporous template owing to the extremely high surface energy of WO_3 molecules compared to that of Au atoms (Figure 5c). In other words, Au nanocrystals have a relatively lower activation energy threshold for rejection from the mesochannels. In fact, experimentally, when the calcination temperature reaches ≈250 °C, the Au nanocrystals are clearly rejected (Figure S10, Supporting Information), while WO_3 can stably exist inside silica mesochannels, even up to ≈600 °C (Figures S12 and S13, Supporting Information).

The discovery that particle-mediated aggregation and mesoscale transformation occurs in ≈10 nm confined mesoporous channels is completely unexpected because the nonclassical crystallization process is based on the OA mechanism, which always involves nanocrystal collision and grain rotation. The calculated results are consistent with the experimental observations. As long as the WO_3 nanocrystals are grown in an oxygen environment, regardless of whether the SiO_2 surface contains absorbed oxygen, WO_3 cluster migration can occur. The initially crystallized fine WO_3 NPs can first diffuse and migrate and become loose aggregates via a particle-mediated OA mechanism since a relatively low activation energy is required. At elevated temperature, atom- or molecule-mediated Ostwald ripening (OR) can be activated. Thus, the obtained loose WO_3 aggregates may further coalesce and densify and finally convert into an ordered dense mesoporous structure. The current OA-driven particle aggregation followed by OR-driven densification is quite similar to the liquid-like nanocrystal growth. In previous investigations into the OA and OR mechanisms, a high internal porosity was frequently observed in the OA process, which originates from unfilled interstices between nanoparticles, while the classical OR process prefers to directly form compact structures via an atom- or molecule-mediated growth approach.[27] Moreover, the OA and OR crystal growth mechanisms can occur simultaneously. In the early stages of the crystal growth, the OA mechanism occurs predominantly. With an extended reaction time, OR can to some extent play a major role in assisting the process of OA in forming the final single crystals.[28] In addition, plane defects, such as multiple twins, delocalization, and stacking faults, are clearly visible in the HRTEM image of the WO_3 networks, as shown in Figure S25 (Supporting Information). This is also a strong indication of WO_3 NP formation through a particle-mediated OA process.[29–33]

In this work, we performed a detailed investigation into growth processes and mechanism for mesoporous-networked WO_3 structures formed within KIT-6 mesochannels using an in situ TEM heating technique, in situ synchrotron SAXS spectroscopy, and DFT calculations. The in situ TEM observations and SAXS measurements indicate that the formation of WO_3 mesostructures involves a particle-mediated mesoscale transformation and coalescence mechanism. First, the initially crystallized, fine WO_3 NPs diffuse, migrate, and form loose aggregates via a particle-mediated OA mechanism. Then, the obtained loose WO_3 aggregates further coalesce and densify, and finally convert into the ordered dense mesoporous structure through an OR-driven mechanism. The liquid-like particle-mediated aggregation and mesoscale transformation process can occur in ≈10 nm confined mesoporous channels, which is completely unexpected. The DFT calculation results are highly consistent with the above observations, in which WO_3 cluster migration occurs more easily than WO_3 molecule detachment from the WO_3 cluster due to the relatively small energy barrier under an oxygen-abundant atmosphere. The detailed mechanistic study will be of great help for experimental design and to exploit a variety of mesoporous materials for diverse applications, such as in catalysis, absorption, separation, energy storage, biomedicine and nanooptics.[34]

Supporting Information

Supporting Information is available from the Wiley Online Library or from the author.

Acknowledgements

This work was supported by the National Natural Science Foundation of China (Grant Nos. 21675122, 51171139, 10434017, and 51501090), the Fundamental Research Funds for the Central Universities (Grant Nos. xkjc2014004 and 30915015103), and the specialized research fund for the doctoral program of higher education of China (Grant No. 20130201110032). We would like to thank D. Y. Zhao for helpful discussion.

Conflict of Interest

The authors declare no conflict of interest.

Keywords

confined spaces, in situ transmission electron microscopy, oriented attachment, particle-mediated mechanisms, small-angle X-ray scattering spectroscopy

Received: July 26, 2017
Revised: September 17, 2017
Published online:

[1] V. K. Lamer, R. H. Dinegar, *J. Am. Chem. Soc.* **1950**, *72*, 4847.
[2] H. Reiss, *J. Chem. Phys.* **1951**, *19*, 482.
[3] Y. N. Xia, Y. J. Xiong, B. Lim, S. E. Skrabalak, *Angew. Chem., Int. Ed.* **2009**, *48*, 60.
[4] R. L. Penn, J. F. Banfield, *Science* **1998**, *281*, 969.
[5] D. S. Li, M. H. Nielsen, J. R. I. Lee, C. Frandsen, J. F. Banfield, J. J. D. Yoreo, *Science* **2012**, *336*, 1014.
[6] H. M. Zheng, R. K. Smith, Y. W. Jun, C. Kisielowski, U. Dahmen, A. P. Alivisatos, *Science* **2009**, *324*, 1309.
[7] H. Colfen, S. Mann, *Angew. Chem., Int. Ed.* **2003**, *42*, 2350.
[8] J. J. De Yoreo, P. U. P. A. Gilbert, N. A. J. M. Sommerdijk, R. L. Penn, S. Whitelam, D. Joester, H. Z. Zhang, J. D. Rimer, A. Navrotsky, J. F. Banfield, A. F. Wallace, F. M. Michel, F. C. Meldrum, H. Cölfen, P. M. Dove, *Science* **2015**, *349*, 6247.
[9] J. X. Fang, B. J. Ding, H. Gleiter, *Chem. Soc. Rev.* **2011**, *40*, 5347.
[10] H. J. You, J. X. Fang, *Nanotoday* **2016**, *11*, 145.
[11] Z. Liu, Z. B. Yang, B. Peng, C. Cao, C. Zhang, H. J. You, Q. H. Xiong, Z. Y. Li, J. X. Fang. *Adv. Mater.* **2014**, *26*, 2431.
[12] J. X. Fang, S. Y. Du, Z. Y. Li, S. Lebedkin, R. Kruk, H. Hahn, *Nano Lett.* **2010**, *10*, 5006.
[13] C. T. Kresge, M. E. Leonowicz, W. J. Roth, J. C. Vartuli, J. S. Beck, *Nature* **1992**, *359*, 710.
[14] D. Y. Zhao, J. L. Feng, Q. S. Huo, N. Melosh, G. H. Fredrickson, B. F. Chmelka, G. D. Stucky, *Science* **1998**, *279*, 548.
[15] H. J. Wang, H. Y. Jeong, M. Imura, L. Wang, L. Radhakrishnan, N. Fujita, T. Castle, O. Terasaki, Y. Yamauchi, *J. Am. Chem. Soc.* **2011**, *133*, 14526.
[16] L. F. Chen, J. C. Hu, R. Richards, *J. Am. Chem. Soc.* **2009**, *131*, 914.
[17] A. T. Delariva, T. W. Hansen, S. R. Challa, A. K. Datye, *J. Catal.* **2013**, *308*, 291.
[18] K. Yoshida, A. Bright, N. Tanaka, *J. Electron Microsc.* **2012**, *61*, 99.
[19] Z. W. Liu, R. C. Che, A. A. Elzatahry, D. Y. Zhao, *ACS Nano* **2014**, *8*, 10455.
[20] G. Prieto, J. Zecevic, H. Friedrich, K. P. de Jong, P. E. de Jongh, *Nat. Mater.* **2013**, *12*, 34.
[21] H. J. Wang, H. Y. Jeong, M. Imura, L. Wang, L. Radhakrishnan, N. Fujita, T. Castle, O. Terasaki, Y. Yamauchi, *J. Am. Chem. Soc.* **2013**, *133*, 14526.
[22] Y. Doi, A. Takai, Y. Sakamoto, O. Terasaki, Y. Yamauchi, K. Kuroda, *Chem. Commun.* **2010**, *46*, 6365.
[23] P. Yang, D. Zhao, D. I. Margolese, B. F. Chmelka, G. D. Stucky, *Nature* **1998**, *396*, 152.
[24] S. Lan, Y. Ren, X. Y. Wei, B. Wang, E. P. Gilbert, T. Shibayama, S. Watanabe, M. Ohnuma, X. L. Wang, *Nat. Commun.* **2017**, *8*, 14679.
[25] S. B. Simonsen, I. Chorkendorff, S. Dahi, M. Skoglundh, J. Sehested, S. Helveg, *J. Am. Chem. Soc.* **2010**, *132*, 7968.
[26] E. D. Martinez, C. Boissiere, D. Grosso, C. Sanchez, H. Troiani, G. J. A. A. Soler-Illia, *J. Phys. Chem. C* **2014**, *118*, 13137.
[27] G. Prévot, N. T. Nguyen, D. Alloyeau, C. Ricolleau, J. Nelayah, *ACS Nano* **2016**, *10*, 4127.
[28] X. G. Xue, R. Lee Penn, E. R. Leite, F. Huang, L. Zhang, *CrystEngComm* **2014**, *16*, 1419.
[29] H. Ataee-Esfahani, S. E. Skrabalak, *RSC Adv.* **2015**, *5*, 47718.
[30] J. S. Chen, T. Zhu, C. M. Li, X. W. Lou, *Angew. Chem., Int. Ed.* **2011**, *50*, 650.
[31] J. W. Nai, B. Y. Guan, L. Yu, X. W. Lou, *Sci. Adv.* **2017**, *3*, e1700732.
[32] J. J. Geuchies, C. V. Overbeek, W. H. Evers, B. Goris, A. de Backer, A. P. Gantapara, F. T. Rabouw, J. Hilhorst, J. L. Peters, O. Konovalov, A. V. Petukhov, M. Dijkstra, L. D. A. Siebbeles, S. van Aert, S. Bals, D. Vanmaekelbergh, *Nat. Mater.* **2016**, *15*, 1248.
[33] M. P. Boneschanscher, W. H. Evers, J. J. Geuchies, T. Altantzis, B. Goris, F. T. Rabouw, S. A. P. van Rossum, H. S. J. van der Zant, L. D. A. Siebbeles, G. V. Tendeloo, I. Swart, J. Hilhorst, A. V. Petukhov, S. Bals, D. Vanmaekelbergh, *Science* **2014**, *344*, 1377.
[34] W. Li, J. Liu, D. Y. Zhao, *Nat. Rev. Mater.* **2016**, *1*, 16023.

